Journal of Hydrology: Regional Studies 52 (2024) 101686

Contents lists available at ScienceDirect

Journal of Hydrology: Regional Studies

journal homepage: www.elsevier.com/locate/ejrh

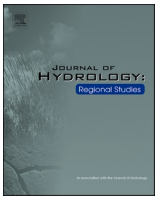

Saltwater intrusion in Chao Phraya Estuary: A long, narrow and meandering partially mixed estuary influenced by water regulation and abstraction

Tanuspong Pokavanich [a,c,*], Xinyu Guo [b]

[a] Department of Marine Science, Faculty of Fisheries, Kasetsart University, Thailand
[b] Center for Marine Environmental Studies, Ehime University, Japan
[c] Center for Advanced Studies for Agriculture and Food, Kasetsart University, Bangkok, Thailand

ARTICLE INFO

Keywords:
Partially mixed estuary
Hydrodynamics
Monsoons
Freshwater abstraction
Numerical model
Sidewall roughness

ABSTRACT

Study area: The Chao Phraya Estuary (CPE) (100° 28'−100° 36'E, 13° 30'−14° 15'N) in the central part of Thailand.
Study focus: To systematically study characters of the CPE, saltwater intrusion and its responses to natural and water regulation and abstraction using high resolution 3D hydrodynamic model with along-the-river measurements.
New hydrological insights for the region: Findings show that: (i) the CPE is a partially mixed estuary regulated by the tide, river discharge, local and remote winds, and seasonal sea level that is substantially influenced by the Asian-Australian monsoon and human factors. (ii) Low freshwater discharge, prevailing down-estuary winds, and the highest annual sea level are the natural causes for the enhancement of estuarine circulation and the greatest saltwater intrusion distance, which both occur in January. (iii) Geometry of the CPE (long, narrow and meandering) enhances the tidal wave energy dissipation through horizontal turbulence and riverbank roughness which should be considered when modelling any similar estuary elsewhere. (iv) Water regulation and abstraction are likely to be responsible for severe intrusion events during 2020 and 2021, which adversely affected more than 14 million people in and around Bangkok. The freshwater discharge rate and saltwater intrusion distance from the river mouth have a negative relation ($R = -0.72$, $p\text{-value} = 0$). Improvement of freshwater allocation within the river basin are primary ways to effectively manage the saltwater intrusion problem.

1. Introduction

Saltwater intrusion is a natural phenomenon in estuaries that is mainly controlled by the river's discharge and tidal range (Prandle, 1985; Simpson et al., 1990; Dyer, 1997; Bowen and Geyer, 2003; Guo and Valle-Levinson, 2007; Zhu et al., 2020). It is also influenced by the estuary's length, width, depth and meandering (Prandle, D, 2006; Chen et al., 2019; Eslami et al., 2019a, 2019b; Wei et al., 2022), river mouth topography (Gong et al., 2022), prevailing winds (Wong, 1994; Guo and Valle-Levinson, 2008; Gong et. al, 2012) and tropical storms (Zhu et al., 2020; Li et al., 2022), as well as sub-tidal currents and sub-tidal sea levels in the outer sea (Wong, 1994; Wongsa, S, 2015; Eslami et al., 2019a, 2019b).

* Correspondence to: No. 50, Ngam Wongwan Road, Lad Yao, Chatuchuk, Bangkok, 10900 Thailand.
E-mail address: ffistop@ku.ac.th (T. Pokavanich).

https://doi.org/10.1016/j.ejrh.2024.101686
Received 10 February 2023; Received in revised form 9 January 2024; Accepted 25 January 2024
Available online 3 February 2024

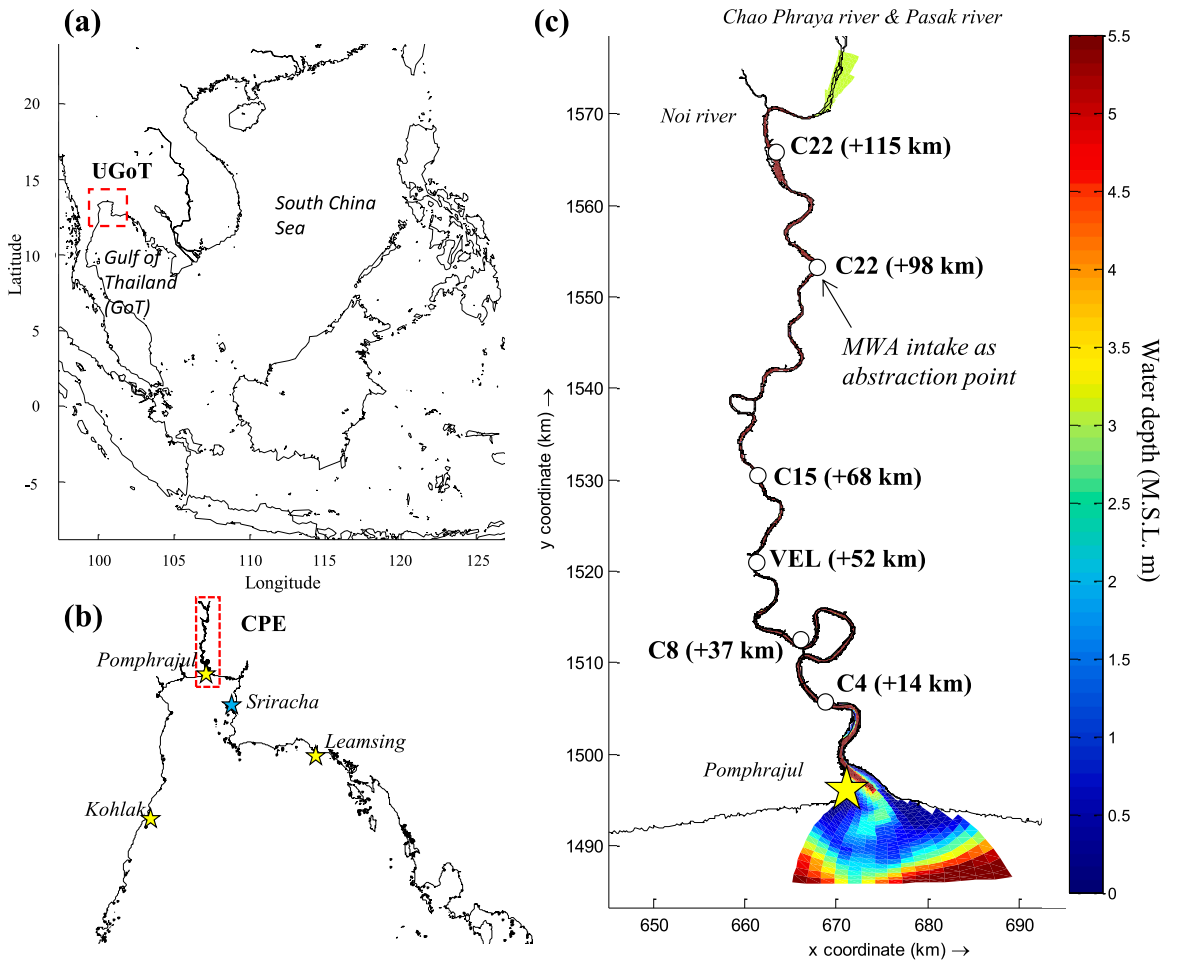

Fig. 1. (a) Location of the Upper Gulf of Thailand. The red box indicates the scale of (b). (b) Location map and topography of the Chao Phraya River Estuary (CPE). Star symbols along the coastline denote tidal gauges. The red box indicates the scale of (c). (c) River channel of CPE and bathymetry. Circle symbols show monitoring stations along the river; their distance from the river mouth is indicated in parentheses.

The combination of these natural forces produces three regimes of the estuary with different salinity structures, i.e., salt wedge estuary, partially mixed estuary, and well-mixed estuary (Pritchard, 1955). The salt wedge estuary mainly exists in weak tidal areas where the estuarine circulation develops with a weak mixing and a sharp halocline. The well-mixed estuary exists in areas where the tidal ranges are large and produce a strong tidal mixing that limits the development of estuarine circulation. In the partially mixed estuary, many factors interplay and cause large changes in the estuarine circulation and saltwater intrusion.

In addition of the natural forces since most cities around the world are located within 250 km of the coastline, human activities may interact with natural forces to alter the physical processes in the estuary, including saltwater intrusion (Liu et al., 2019; Wei et al., 2022). For example, modification of the river topography by sand mining and land reclamation causes the tidal wave to travel further upstream and also enhances saltwater intrusion (Zhang et al., 2010; Shen et al., 2018; Chen et al., 2019; Eslami et al., 2019a, 2019b). Modification of vegetation along the river through city development can affect flow fields through modification of the flow resistance (e.g., Pettit et al., 2016; Errico et al., 2019; Crimaldi and Lama, 2021). Civil engineering structures for water control and treatment of storm surges affect freshwater discharge and length of the estuary, which also alter the tidal propagation and the saltwater intrusion distance (Ding et al., 2021; Ralston et al., 2022; Wei et al., 2022). Furthermore, climate change and global sea level rise can increase saltwater intrusion in low-lying estuaries (e.g., Wongsa, S, 2015; Eslami et al., 2019a, 2019b).

The Chao Phraya River Estuary (CPE) is a good example of a populous estuary. It is a vast, flat and very low-lying area surrounded by agricultural areas, cities, and industrial areas. It is situated in the central region of Thailand (Fig. 1). The Chao Phraya River is one of the largest rivers in Southeast Asia, and the river's path is narrow, long, and meandering. The river has a wide but shallow mouth, and its estuary would be expected to be partially mixed considering the tidal range and river discharge. However, to date, there have been no studies or sufficient evidence to confirm this. Vongvisesssomjai and Chatanantavet (2006) developed an analytic model to describe tidal and river discharge fluctuation at several locations along the river. Sirisup et al. (2014) used a two-dimensional hydrodynamic model to investigate the variation of water level and tidal flow velocity along the river. Wongsa (2015) and Chettanawanit (2021) used

Table 1
Major water regulation and abstraction infrastructures of the Chao Phraya River.

Name of the infrastructure	Location	Operational year	Purpose
Sirikit dam	17°52.80′N, 100°27.72′E	1971	Water storage and electricity generation
Bhumipol dam	17°15.90′N, 100°54.00′E	1964	Water storage and electricity generation
Chao Phraya Diversion dam	15°9.55′N, 100°10.78′E	1957	Flood control, irrigation and electricity generation
Rama VI Diversion dam	14°33.52′N, 100°45.68′E	1924	Flood control and irrigation
Samlae Raw Water Pumping Station (MPA intake)	14°2.49′N, 100°33.30E	1914	Water abstraction as raw water for the MPA.

a one-dimensional hydrodynamic model to quantify the effects of sea level rise and freshwater abstraction on saltwater intrusion in the CPE. Changlkom et al. (2022) combined multiple linear regression and artificial neural networks to make a 1–5 day prediction of salinity at the raw water intake of Bangkok's Metropolitan Waterworks Authority (MWA) based on the water level at an upstream location.

In recent years, the CPE has experienced severe saltwater intrusion events, during which the raw water intake of MWA was contaminated by water with salinity higher than (0.25–0.50 PSU) more frequently than in the past and for a longer duration, e.g., more than 3 months in 2020 and 4.5 months in 2021 (Wongsa, 2015; Chettanawanit et al., 2021; Changklom et al., 2022). This is even though the MWA's raw intake is considerably far from the river mouth (approximately 98 km from the river mouth, hereafter "+98 km"). The severe saltwater intrusion will affect people's health (Changklom et al., 2022), contaminate soil, and cause crop harvest reduction (Phankamolsil, et al., 2021) and economic loss on a wide scale. Combatting the saltwater intrusion problem therefore is a national priority, however, none of the previous studies described the hydrodynamics and saltwater intrusion in the CPE in adequate detail to combat the problem (Bidorn et al., 2021; Changklom et al., 2022).

In this study, we first report the overall dynamics of the CPE in response to natural factors by using data from field observations and results of a three-dimensional numerical model. While the modeling may not fully represent various aspects of the real world due to its reliance on assumptions and simplified input data (e.g., Chen et al., 2019; Errico et al., 2019; Zhu et al., 2020; Gong et al., 2022), numerical modeling remains the most practical method for initially exploring the interplay between natural and anthropogenic influences affecting hydrodynamics and salt intrusion in the CPE. Additionally, we provide an explanation of the mechanisms for the severe saltwater intrusion in recent years, which is likely associated with freshwater discharge modification by water engineering structures, water regulation along the river and water abstraction for irrigation and cities. Our study illustrates that not only natural factors but also human activities are important to the populous estuarine system. Our findings can be applied to the management of water resources in the CPE and other partially mixed estuaries.

2. Materials and methods

2.1. Study site

The CPE (100° 28'−100° 36'E, 13° 30'−14° 15'N) is one of the most important lands for rice production and is the most populous area in Thailand that has the Chao Phraya River as the main river. The CPE has a drainage basin area of approximately 160×10^3 km^2. The river is the largest in Thailand and one of the largest rivers in Southeast Asia (Saito, 2001). The river has an annual mean discharge of 480 m^3/s (70-year average) and monsoonal variation producing a range of about 100 m^3/s to 2400 m^3/s (Bidorn et al., 2021). The CPE is situated in the central part of Thailand and its land elevation is approximately 0.5–1.5 m above mean sea level (Trisirisatayawong et al., 2011). This low elevation has been subject to a substantial rate of land subsidence during the past decades (Trisirisatayawong et al., 2011; Saramul and Ezer, 2014).

The Chao Phraya River is an important source of freshwater for agriculture, industries, and cities including the metropolis of Bangkok, where more than 14 million people live. During recent decades, the demand from these domestic, industrial, agricultural, and environmental sectors for freshwater has increased (Molle et al., 2001; Phankamolsil, et al., 2021; Changklom et al., 2022), while the water quality of the CPE has continued to decline (Horiuchi et al., 2020). There is a long history of the development of irrigation and navigation canals as well as gates and dams for water regulation within the estuary (See Table 1). The lower CPE (from the river mouth to approximately +70 km) is heavily used for river transportation and therefore has many engineering structures along the riverside. Consequently, this area is sometimes called the "Venice of the East."

The freshwater resource supplied by the CPE is very limited during the dry season (December to June) due to many competing demands from a variety of sectors (Molle et al., 2001; Chettanawanit et al., 2021; Phankamolsil, et al., 2021; Changklom et al., 2022). The amount of freshwater varies inter-annually as a response to major climate phenomena such as El Niño–Southern Oscillation (ENSO), the variability of sea surface temperature (SST) over the tropical Atlantic, the Pacific decadal oscillation (PDO), and the Indian Ocean dipole mode (IOD) (Cai et al., 2019, 2021; Phan-Van et al., 2022). As reported by the Bureau of Meteorology, Australian Government during the period of 2018–2019 overall rainfall intensity at Australia and Southeast Asia was low following the modulate El Niño period. In 2020, the rainfall intensity increased due to La Nina. Therefore, freshwater discharge at CPE was limited in the year 2020 but large in the year 2021 which will be called hereafter "dry year" and "wet year", respectively.

Similar to estuaries elsewhere, the saltwater intrusion problem is mitigated by the release of freshwater from upstream dams to push the saltwater toward the sea (e.g. Zhu et al., 2020, Payo-Payo et al., 2022), although this is only possible if there is sufficient stored water. As reported by the water regulators in Thailand, the situation in the CPE is made more complex because the salinity

values does not respond linearly to the amount of released freshwater.

2.2. Topography of the CPE

The CPE was formed as a drowned river valley type estuary (Dyer, 1997). This low-lying, long and narrow estuary has a shallow river mouth with an average depth of ~2.3 m. At the seaward side of the mouth, there are two navigational channels with a depth of ~7 m and width of ~300 m connecting the CPE to the Upper Gulf of Thailand. From the river mouth to + 120 km upstream, the CPE has an average depth of 8.75 m. In this reach, there are a few deep pools where the water depth is greater than 30 m, and were produced by river sand mining in the past.

The width of the river mouth is approximately 6 km, but this is reduced rapidly within the estuary. The average width in the reach below + 15 km is ~2 km and ~300 m above this point. The minimum width is ~140 m at approximately + 50 km. From the mouth to + 120 km, the CPE has a volume of about 1.03 km^3 and the tidal prism (i.e., the difference in volume of water between high tide and low tide) is ~ 0.15 km^3 and ~0.24 km^3 in neap and spring tides, respectively.

2.3. Available measured data

We collected hourly data of water level, salinity, river discharge and wind within the CPE. The water levels, salinity and water temperature at stations C4 (+15 km), C8 (+35 km), C15 (+70 km) and C22 (+98 km) (Fig. 1c) were provided by the Metropolitan Waterworks Authority (MWA). In addition, we collected hourly water level data from the Hydrographic Department (HD), Royal Thai Navy near the river mouth (station Pomprajul, 13°9.850′N, 100°54.385′E, Fig. 1c), and at offshore locations about 180 km southwest of the river mouth (station Koh Lak, 11° 47.700'N, 99° 48.967'E, Fig. 1b) and about 200 km southeast of the river mouth (station Leam Sing, 12° 27.804'N, 101° 57.682'E, Fig. 1b). An acoustic Doppler current profiler-measured river flow velocity at 10-minute intervals from station VEL at + 50 km (Fig. 1c) was also provided by the HD. River discharge data at 15-day intervals were obtained from the Royal Irrigation Department (RID) website (http://water.rid.go.th/flood/plan_new/planlow.html, accessed on 1 September 2022). Wind data at station Sriracha (13°11.137'N, 100°55.086'E), an online marine observation station located about 50 km southeast of the river mouth (Fig. 1c), are from the Hydro-Informatics Institute (HII). River mouth area bathymetry data was derived from navigational charts of the HD and inside the river data was provided by the Marine Department (MD). All the measurement data were quality controlled by manually removing an obvious spikes and error data, box-averaged or filtered using Butterworth low-pass filter before their usages and plots with Microsoft Excel program.

Field surveys to collect Conductivity-Temperature-Depth measurements using AAQ-RINKO171 (JFE Advantech, JAPAN) were carried out at 29 stations along the river's longitudinal axis from the river mouth to + 120 km at several times: in a drought year on 28 February 2021 (spring tide) and 7 March 2021 (neap tide); and in a wet year between 30 November 2021 and 27 February 2022, with 7 consecutive neap tides and 1 spring tide. The surveys were carried out with a speed boat and each survey required roughly 5–9 h. After removing an obvious error manually, we averaged the measured data as 10-cm vertical cells before plot with contour function using MATLAB program.

2.4. Numerical model

A three-dimensional hydrodynamic model for the CPE was configured using Delft3D-FLOW (Deltares, 2017) model with a domain from 30 km offshore of the CPE's river mouth to + 180 km (Fig. 1c). Model grids are arranged in a curvilinear coordinate system. There are 14 sigma layers in the vertical dimension, with thickness of 5,6,7,8,8,8,8,8,8,8,8,7,6,5% of the total depth from the sea surface to the sea bottom, respectively. The horizontal grid has a minimum cell size of approximately 40 × 40 m^2 in the area close to the salt-water front between + 15 to + 40 km. The grid cell size slowly increases upstream and downstream from this zone. The grid is artificially expanded at the upstream end to have larger water volume than actually exists in the CPE to compensate for the water volume of surrounding irrigation channels, which are ignored in this study. Determining upstream grid size of the model were parts of the model calibration process. This adjustment is essential for the realistic water level reproduction of the model, as it has been reported that the presence of an irrigation system along the river can reduce the tidal amplitude by up to 25% (Eslami et al., 2019a, 2019b).

At the upstream boundary, the freshwater discharge data from the RID with a 15-day interval for the Chao Phraya River and Pasak River (95% of the total discharge into the CPE) and Noi River (5% of the total discharge) were applied. At the location of the MWA's raw water intake (+98 km), a constant amount of − 55 m^3/s was withdrawn (based on 2021 field measured data and data provided by the MWA). At the offshore lateral boundary, the hourly water level data from the HD at station Pomprajul were specified. The measured wind speed and direction data at station Sriracha from the HII (see Fig. 1b for its position) were used to calculate the wind stresses that were treated as spatially homogenous in the model domain. The drag coefficient used in the quadratic formula for wind stresses follows Smith and Banke (1975). The model estimates turbulence parameters using the horizontal large eddy simulation (Vossen, 2000) and k-ε model for the horizontal and vertical turbulence, respectively. The Prandtl number is 1. Roughness values at the sidewall follow the logarithmic law of the wall. The bed shear stress uses a quadratic bed stress formula. The model was run from a rest state with an initial salinity of 0 and a time step of 30 s. The simulation period is from October 2020 to March 2022, which covers dry and wet periods.

We wanted to use the model to reproduce the spatial distributions of water level, flow velocity, and salinity for both intra-seasonal and seasonal variations in the CPE. The model was parameterized for the best reproduction of water level, flow velocity, and salinity.

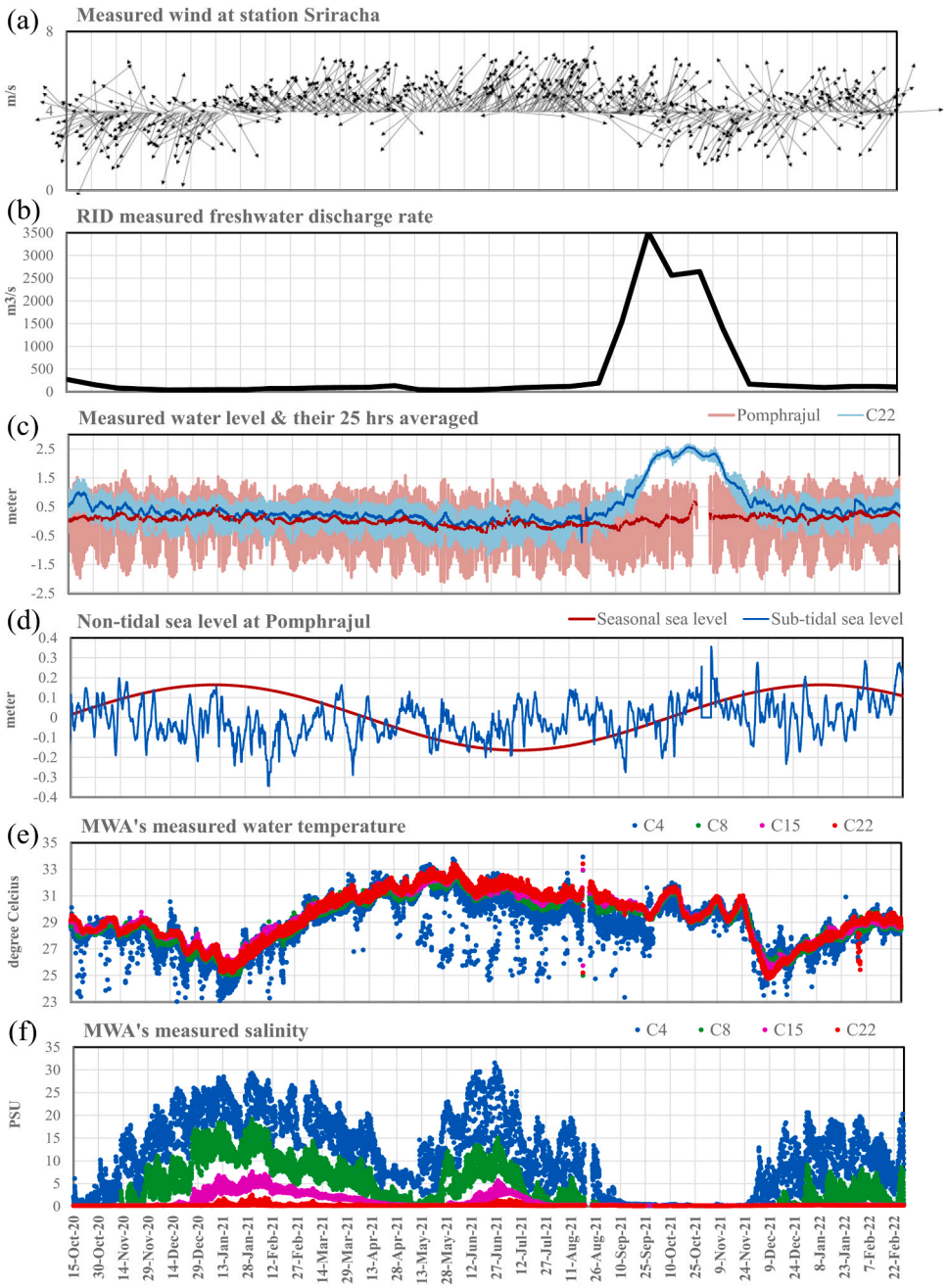

Fig. 2. Time series of (a) measured wind at station Sriracha, (b) river discharge from global rainfall-runoff model (blue line) and that reported by the Royal Irrigation Department with some modifications (black line), (c) water levels measured at stations Pomprajul and C22, (d) sub-tidal water level and seasonal sea level variation data derived from measurements at station Pomprajul, (e) and (f) water temperature and salinity, respectively, measured at stations C4, C8, C15 and C22. Time spacing in horizontal axis is 15 days.

During the tuning of the model, the model grid, background horizontal and vertical eddy viscosity, bottom roughness, wind drag coefficient, sidewall roughness, and freshwater discharge were modified step by step. Best results were obtained from the model configuration using an expanded tail grid, zero background eddy viscosity, 4 m of the sidewall, spatially varying bottom roughness with the Chezy values between 65–130 $m^{1/2}/s$, and wind drag coefficients of 0 and 0.004 at wind speeds of 0 m/s and 25 m/s, respectively. Applying spatially varying Chezy values aims to consider the natural variation in bottom roughness caused by riverbed characteristics and vegetation (Errico et al., 2019; Crimaldi and Lama, 2021).

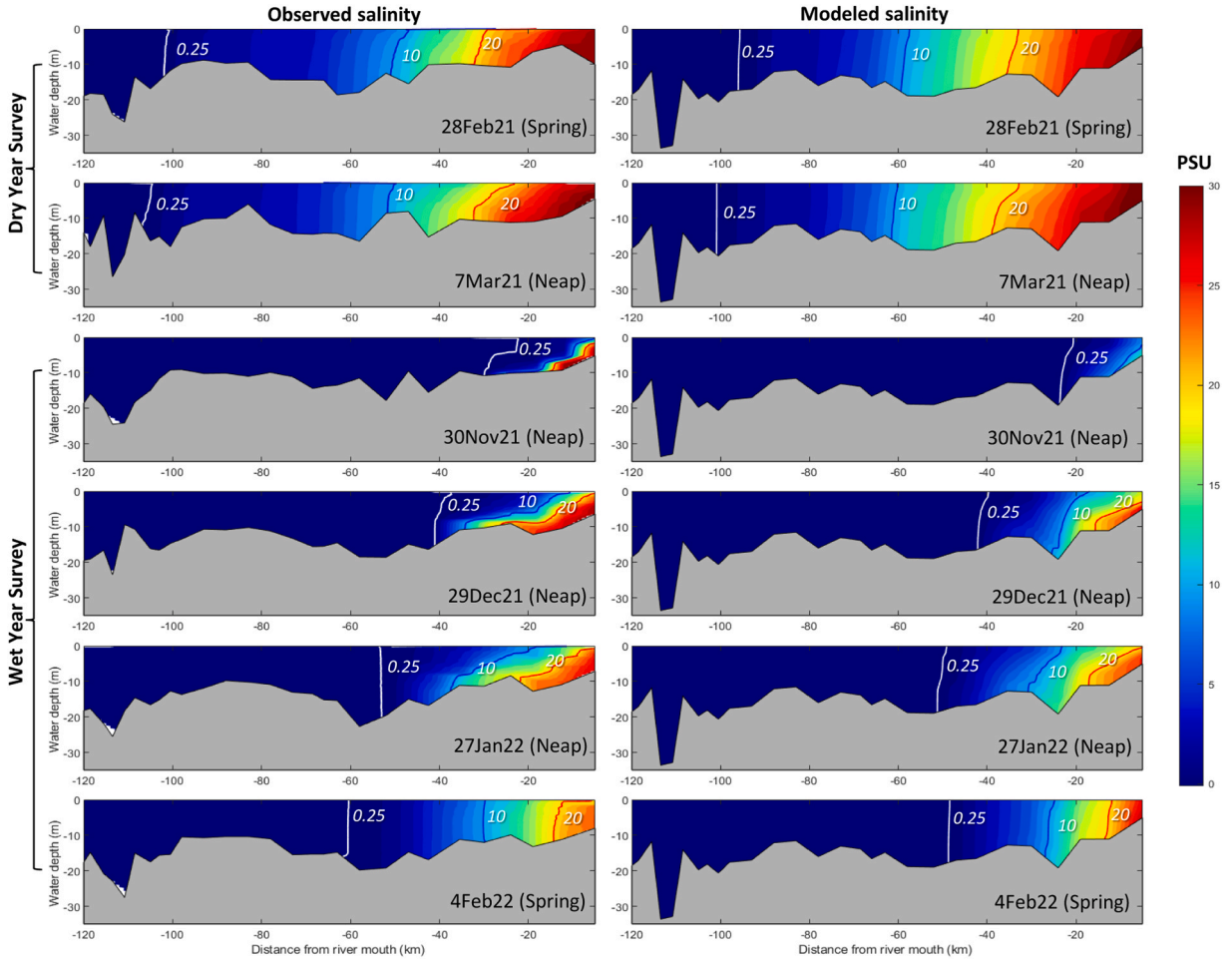

Fig. 3. Observed (left panels) and simulated (right panels) salinity along longitudinal section in the dry year from February to March 2021, and in the wet year from November 2021 to February 2022. Red, blue and white lines represent salinity of 20, 10 and 0.25 PSU.

3. Results and discussion

3.1. Observed results

Time series of some of the data collected over 500 days between October 2020 and February 2022 are shown in Fig. 2. Wind data indicate two prevailing winds, namely the northeasterly from mid-October to mid-January and the southwesterly during the other parts of the year. Freshwater discharge varies seasonally in which it is naturally low in the "dry season" (< 150 m^3/s) during mid-November to mid-June. By nature, the discharge increases greatly in the "wet season" during July to September corresponds to the period of the southwesterly wind. Therefore, it can be seen that wind and freshwater discharges of CPE are closely associated with the monsoon. The dry season occurs during the northeast monsoon (NEM) and the transition from the NEM to the southwest monsoon (SWM). The wet season occurs during the SWM. Peak discharges typically appear at the end of the SWM, typically in October. Along the river, freshwater is always being abstracted for irrigation and utilization by cities. At station C22 (see Figure1), a constant amount of freshwater is abstracted by the MWA.

As shown by measured water level, although the CPE has a narrow and shallow mouth, tides can travel upstream to about + 250 km. Tidal range varied widely in the CPE, with a maximum value of about 3.6 m at the river mouth (station Pomphrajul in Fig. 2c) but a much smaller value of 1.6 m at + 98 km (station C22, Fig. 2c). With such large reduction of tidal range toward the head of the estuary, the CPE can be classified as a hyposynchronous estuary, where the friction exceeds the effects of convergence (Dyer, K, 1997). At the river mouth, tides are governed by M_2, S_2, O_1, K_1 tidal constituents, for which the amplitudes were 0.55 0.25, 0.41, 0.64 m, respectively. The Formzahl number (K1 +O1)/(M2 +S2) has a value of 1.31, which is consistent with a previously reported value (Saramul and Ezer, 2014). Overall mean water levels within the CPE are higher than on the seaward side. During the wet, the tidal influence on water level in the CPE is significantly reduced. Comparison between the measured water levels at station C22 and station Pomphrajul shows that the water level at the upstream site notably increases during the high river discharge time, but shows

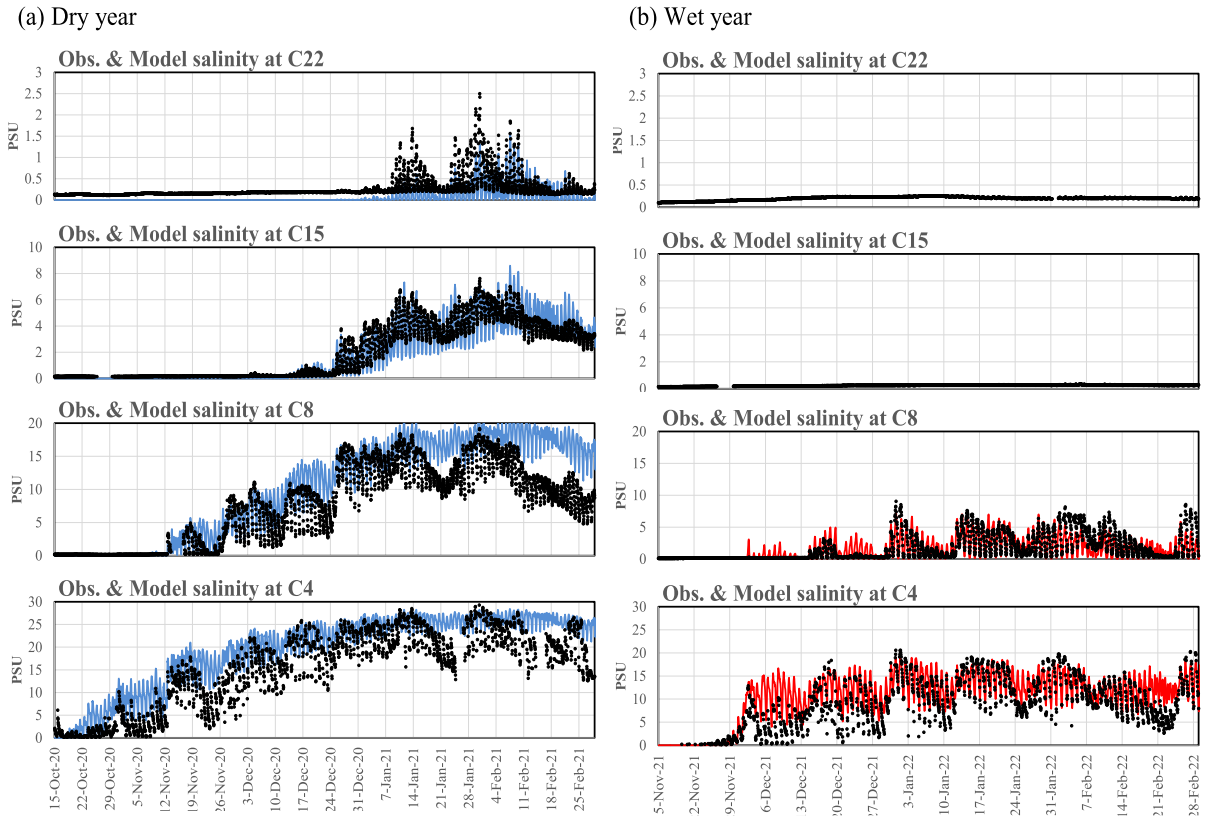

Fig. 4. Observed (black dots) and simulated (blue line or red line) salinity at stations C4, C8, C15 and C22 (a) from October 2020 to February 2021 (dry year) and (b) from November 2021 to February 2022 (wet year).

less tidal variation (Fig. 2d). On the other hand, the water level at the river mouth changes little during the high river discharge time.

In addition to tides, the water levels recorded at station Pomprajul reveal sub-tidal sea level variations, with a maximum value of ~0.3 m and a period of 2–7 days (blue line in Fig. 2d). Seasonal variation with a magnitude of ~0.2 m also appears at the river mouth (red line in Fig. 2d), where the sea level increases during the NEM period but decreases during the SWM period. The highest sea levels occurred in January while the lowest were in June, consistent with previous reports (Saramul and Ezer, 2014; Higuchi et al., 2020, Qu et al., 2022).

Considering the hydrographic data, since the observed water temperature (Fig. 2e) shows little spatial variation among the four stations, we therefore focus on the salinity hereafter. Salinity records at the four stations indicate a complex pattern with both slow and rapid changes in values associated with tidal and subtidal signal (Fig. 2f). The salinity varied significantly (>5 ppt) within periods of one day (diurnally), and the variation was larger during the spring tide compared to the neap tide. Salinity also showed increasing and decreasing trends over periods of 14 days (fortnightly) as well as by month and season. The salinity changes inversely with the river discharge. Salinity measurements at station C22 (+ 98 km), which is the location of the MWA's raw water intake, indicate that the salt intrusion contaminated the municipal water with salinity higher than 0.25 PSU (i.e., the standard for drinking water) for the period from December 2020 to March 2021, and again in June 2021. Observed distribution of salinity along the longitudinal section of the CPE are shown in following section.

3.2. *Model validation*

The model was able to reproduce water level, flow velocity and salinity at locations along the CPE with acceptable accuracy spatially and temporally. The model was also able to reproduce some of the spatial variation in salinity along the river channel corresponding to the wet and dry years and to the neap and spring tides (Fig. 3). For example, the model results show a deeper intrusion of saltwater into the CPE in the dry year (when salinity 10 ppt were recorded as far as +50 km) relative to wet year (when salinity 10 ppt were recorded as far as +30 km). The model was able to reproduce the well-mixed salinity distribution in spring tide but stratified structure in neap tide, which is similar to our observations. Temporally, water levels at station C8 and C22, were reproduced when compare with the measured data with Root-Mean Square Error (RMSE) = 0.19 and 0.13 m; Mean Absolute Error (MAE) = 0.13 and 0.09 m; Coefficient of determination (R2) = 0.93 and 0.90, respectively. At station VEL, the model can reproduce flow velocity in principle direction with RMSE = 0.19 m/s, MAE= 0.15 m/s and R2 = 0.88. During the transition period between wet and dry season,

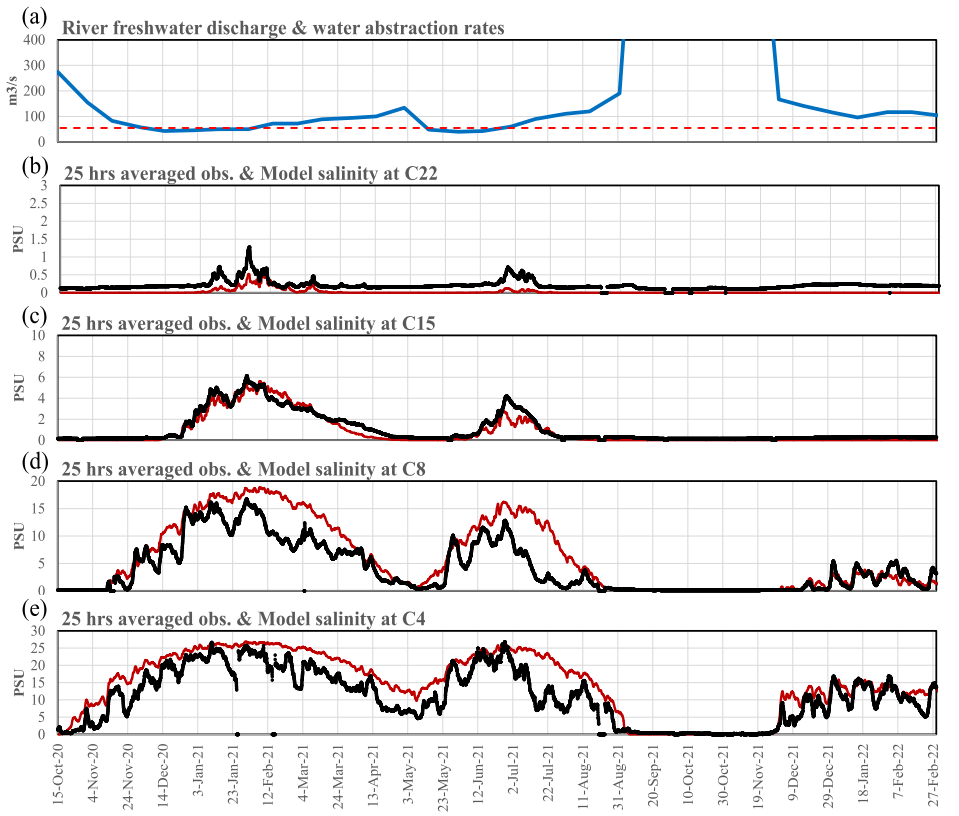

Fig. 5. Inter-seasonal comparison between (a) reported freshwater discharge by the Royal Irrigation Department with some modification to improve the model's reproducibility of salinity distribution (blue line) and WMA's freshwater abstraction rate (red line) and 25-hour low-pass filtered salinity from the observation (black line) and the model results (red line) at stations C4(b), C8(c), C15(d) and C22(e).

the model reproduces salinity at station C4, C8, C15 and C22 with good degree of agreement when compared to the measured data both in the dry year and wet year. In the dry year, the model reproduce salinity with the RMSE = 5.84, 4.06, 0.58 and 0.28 PSU; the MAE = 4.79, 2.87, 0.41, and 0.22 PSU; the R2 = 0.82, 0.83, 0.90 and 0.51, respectively. In the wet year, the model reproduce salinity with the RMSE = 3.34, 1.00, 0 and 0 PSU; the MAE = 2.46, 0.63, 0, and 0 PSU; the R2 = 0.76, 0.71, 1 and 1, respectively..

The model was also run across a long time span (i.e., from October 2020 to February 2022) to confirm the model's performance in representing seasonal salinity variation. Good reproduction of the spatial and temporal changes in salinity was achieved with a slight modification of the RID's freshwater data, which has an interval of 15 days. Fig. 5a shows the final river discharge and freshwater abstraction by the MWA and a comparison of modelled and observed salinity at several stations. Importantly, the model was able to reproduce the peculiar decrease/increase of salinity during the dry season in the dry year (February to June 2021). Fig. 5b, c, d and e show comparison between the modelled salinity and measurement as 25-hours low-pass filtered values with the RMSE = 0.21, 0.44, 3.39 and 5.09 PSU; the MAE = 0.18, 0.33, 2.18 and 4.04 PSU; the R2 = 0.61, 0.94, 0.84 and 0.85 at station C22, C15, C8, C4, respectively.

3.3. Responses of the CPE to its geometry

During the model set-up and calibration, we found that the model results were sensitive to the selection of horizontal eddy viscosity and side wall roughness. Their values significantly affect water level variation along the CPE and their influence increases with distance from the river mouth. To investigate this, we compared three simulation cases, which used best model parameterization (=Case1), set side wall roughness to 0 in Case 1 (=Case2), and reduced turbulence in Case 1 (=Case 3). In Case 3, we set the horizontal turbulence to be equal to the vertical turbulence calculated from the k-epsilon model.

The calculated amplitude and phase of the tidal level, the amplitude of the tidal current, and the salinity along the CPE in three cases are shown in Fig. 6. The amplitude of tidal level significantly increases at locations away from the river mouth in Cases 2 and 3 as compared with Case 1. Such effects are more apparent for the diurnal tides than for the semi-diurnal tides. An increase in tidal level causes a significant increase in flow velocities as well, which is also more apparent for the diurnal tides than for the semi-diurnal tides. The salinity distribution along the river suggests an enhanced seawater intrusion attributable to much greater tidal mixing in Cases 2 and 3.

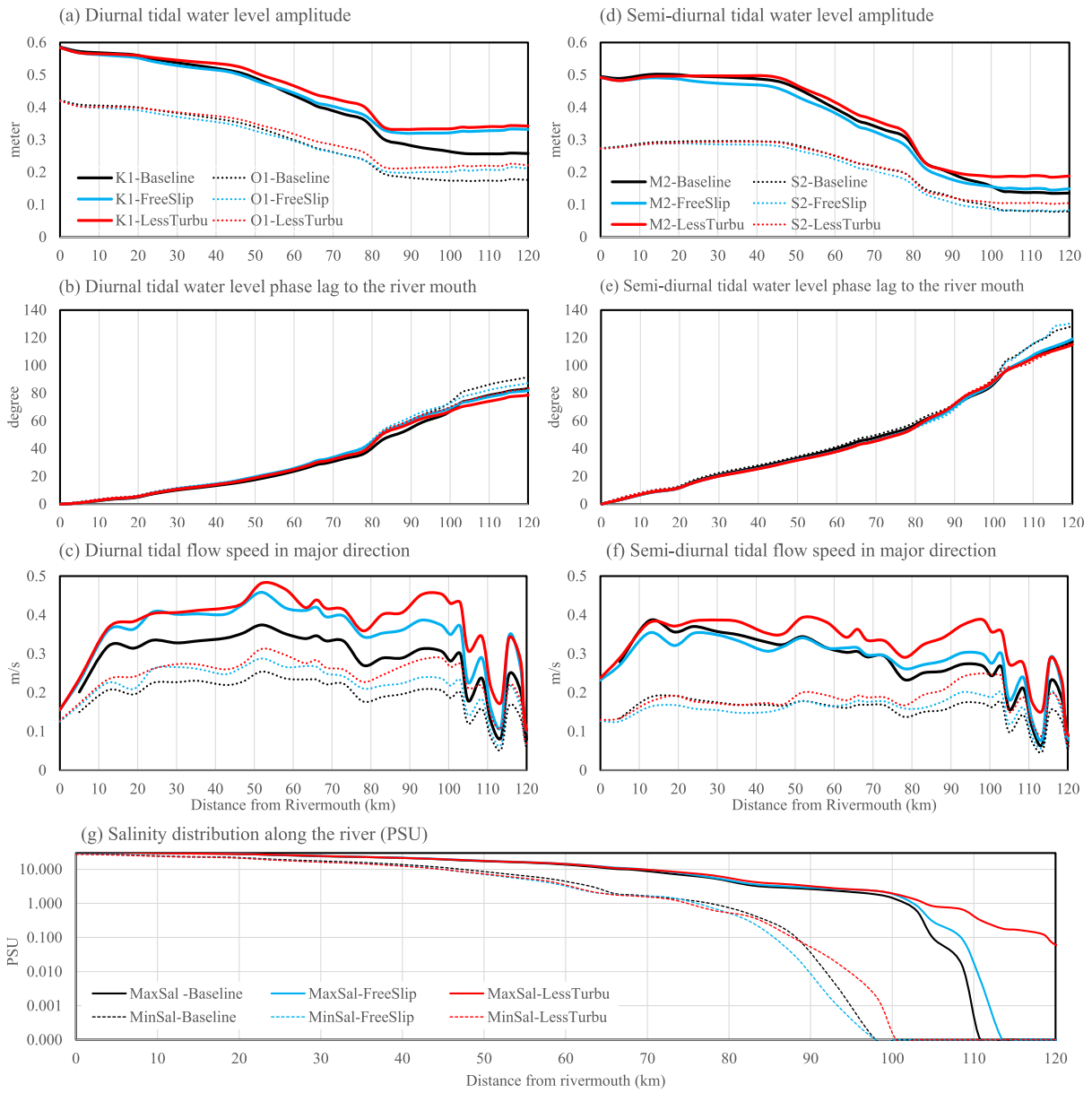

Fig. 6. Comparison between simulation using best model parameterization (Case 1), simulation with free slip at sidewall (Case 2), and simulation that sets the horizontal turbulence to be equal to the vertical turbulence (Case 3). Tidal amplitudes of (a) diurnal (O_1&K_1) and (b) semi-diurnal (M_2 &S_2) constituents, tidal phases from the river mouth of (c) diurnal (O_1&K_1) and (d) semi-diurnal (M_2 &S_2) constituents, amplitudes of surface tidal current in the major direction of diurnal (O_1&K_1) and semi-diurnal (M_2 &S_2) constituents, (g) maximum and minimum near-surface salinity along the longitudinal axis in the CPE.

Such significant effects of the side wall and horizontal turbulence parameters on water level and velocity in estuaries and other water bodies have not been previously reported. In our case, the horizontal turbulence might be elevated due to the geometry of the CPE, which is long and narrow. Meandering of the CPE causes a complex flow field with centrifugal force that creates a secondary flow and the appearance of asymmetry between flood and ebb currents, all of which increase the velocity gradients and the horizontal turbulence. Such effects are less pronounced in wide and relatively straight estuaries (Pein et al., 2018). Although the effects of the side wall can be generally ignored in any non-laboratory scale simulation (Deltares, 2017), it is likely important in a long and narrow estuary where the upstream water level and flow velocity depend strongly on the amount of energy dissipation from the tidal waves at the region near the river mouth. Using a curvilinear grid along the river bank with resolution that is too coarse, the side wall friction and associated sub-grid scale turbulence caused by river bank irregularities can be underestimated. Therefore, it is better to increase the side wall roughness to compensate for this effect when modelling a narrow and long estuary.

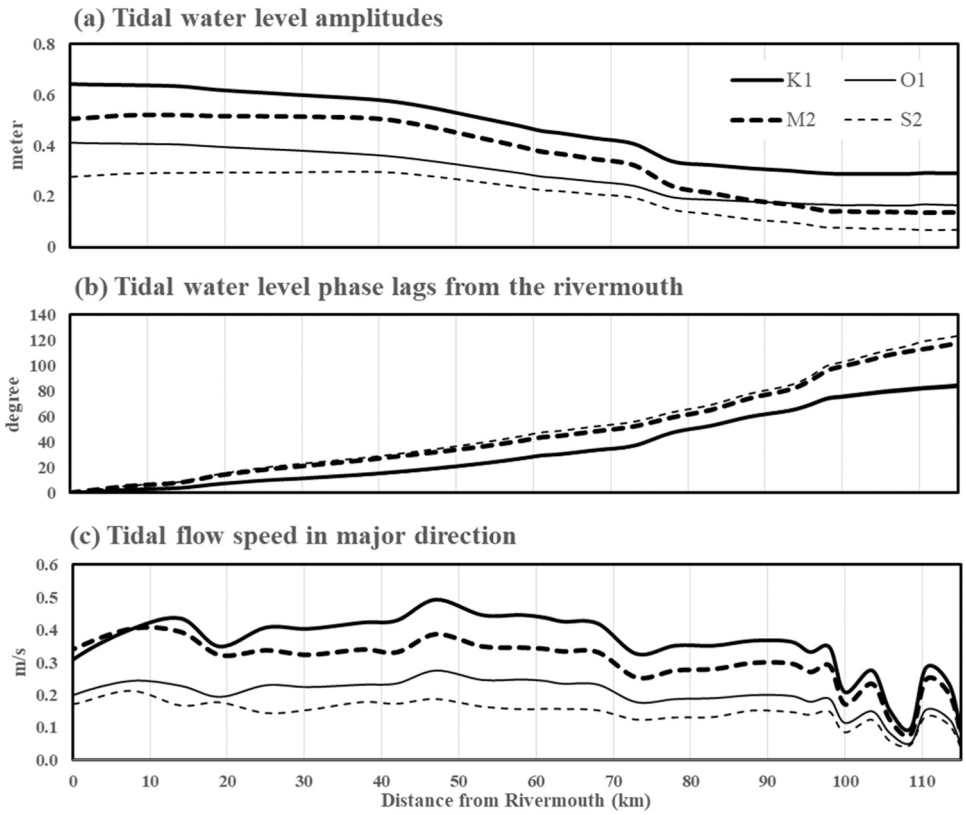

Fig. 7. (a) Tidal amplitudes, (b) tidal phases from the river mouth, (c) amplitudes of surface tidal current in the principal direction of the major diurnal (O_1&K_1) and major semi-diurnal (M_2 &S_2) constituents along the longitudinal axis of the CPE.

3.4. Responses of the CPE to tides

We show the major diurnal and semi-diurnal components of tide and tidal currents along the CPE up to + 120 km in Fig. 7. The tide and tidal flow are found everywhere in our model domain. Tidal water levels diminish along the upstream direction, and tidal waves penetrate upstream from the sea. Compared to diurnal tides, the phase of semi-diurnal tides changes more along the river channel. Tidal flow is weaker upstream than near the river mouth. K_1 and M_2 tides contribute most to the flow velocity in the major direction (i.e., parallel to the river's longitudinal axis) (Fig. 6c). The restricted mouth of CPE causes highest flow velocities in that area. The highest velocity of tidal flow appears between + 10 km and + 50 km and decrease toward upstream direction. This is characteristic of hyposynchronous estuaries (Dyer, 1997) when energy dissipation is larger than the flow convergence. The flow velocity is altered rapidly along the river channel due to irregularities in width and depth. With such a large range of tides, the tidal currents naturally dominate in the CPE (figure not shown). Near the mouth, the flood current and ebb current reach maximum speed (>0.9 m/s) about 4–5 h before the high tides and low tides, respectively. The average phase lag between flow velocity and water level is about 40–50 degrees. This value is neither close to 90 degrees as in a pure standing wave (S) nor to 0 degrees as in a pure progressive wave (P), suggesting that the tidal wave in the CPE is an S+P type (Dyer, K, 1997).

Salinity varies also with tidal phase. Although not shown here, field observations and model results indicate that the diurnal highest salinity occurs at the end of the flood tide, while the lowest salinity occurs at the end of the ebb tide. During ebb tides, the vertical structure of salinity becomes clear and the water stratification is especially strong during neap tides. During flood tides, strong inflow of tidal currents thoroughly mix the water column and the salinity becomes homogenous vertically. Yang et al. (2017) reported that this response is associated with tidal straining in which the vertical shear of the fluctuating tidal current affects the horizontal density gradient, and hence the vertical distribution of salinity. The fortnight change of tidal flow induces an alternation between the stratified and well-mixed structure of salinity in areas near the river mouth (Fig. 8). The neap tide allows the water column to be more stable, which in turn allows intensification of the estuarine circulation in the CPE. At station C4, the estuarine circulation causes the near-surface layer to flow out into the sea and the sub-surface layer to flow in (Fig. 8). Stronger inflowing currents in the lower layers are associated with marked salinity increase. This process causes rapid increase in salinity along the river. The correlation between salinity and flow velocity in the principal direction in the bottom layer after applying the 25-hours low-pass filter was significant ($R = 0.89$, *p-value = 0*).

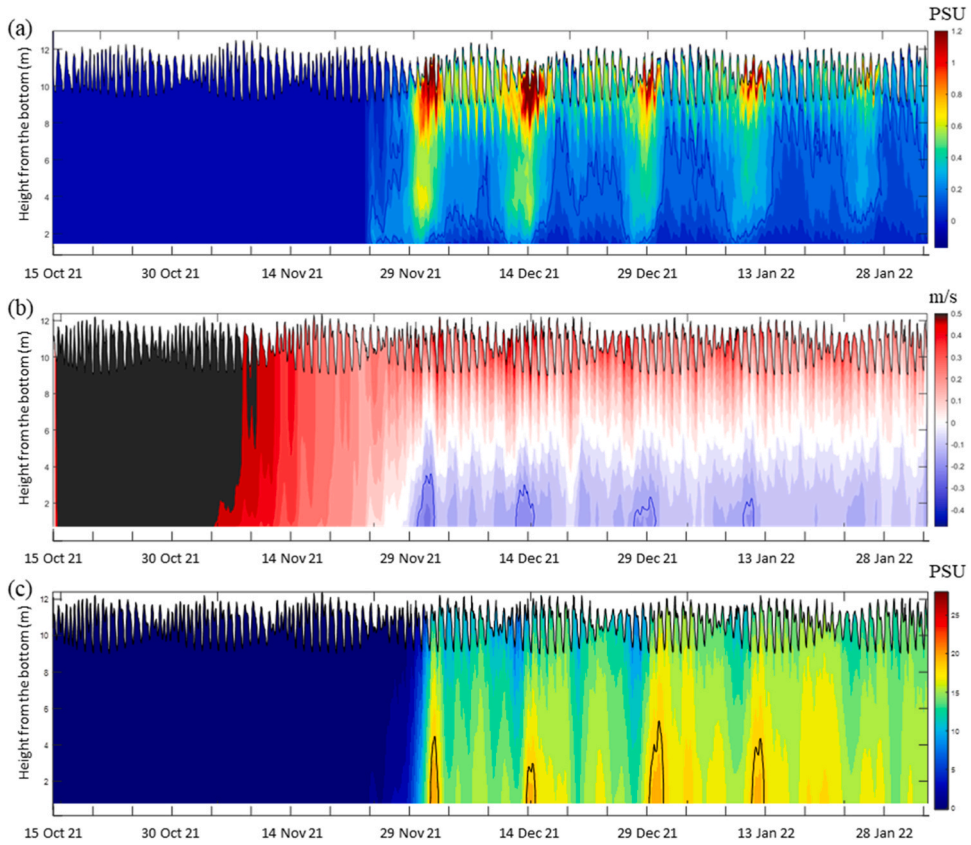

Fig. 8. 25-hr low-pass filtered model results at station C4: (a) vertical gradient of salinity, where color tone represents salinity gradient (PSU/m) and blue line represents 0.5 PSU/m; (b) flow velocity in main direction, negative values indicate downstream direction and positive values indicate upstream, blue contour line indicates value of − 0.14 m/s; and (c) salinity, where color tone has a salinity range of 0–28 and the black line near the bottom represents 19 PSU. The sea surface (black line in each panel) has a clear fortnight variation with a range of 2.5 m.

3.5. Responses of the CPE to winds

The variation in winds that impact the CPE follows the weather pattern of the upper Gulf of Thailand, which is strongly controlled by the Asian-Australian monsoon (Bidorn et al., 2021; Wang et al., 2021; Buranapratheprat et al., 2008). The winds affect the CPE locally and remotely. To investigate the local wind effects, we ran two simulations, with and without winds, for the period of 1 December 2021 to 31 January 2022 using the same river discharge and offshore tidal variations. Differences between the two cases, in terms of 25-hr low-pass filtered flow velocity in principal direction and salinity at station C3 and C4 are shown in Fig. 9.

A northeasterly (down-estuary) wind dominates in the first half of the simulation (Fig. 9a) and induces a strong outflow in the surface layer and a strong inflow in the middle and bottom layers (Fig. 9b and d). The enhanced estuarine current likely increases the seawater intrusion and hence gives a positive value in salinity difference (Fig. 9c and e). The east or southeast winds dominate the second half of the simulation (after 5 January 2022), causing surface water to flow upstream, and therefore weaken the estuarine circulation. Consequently, the intrusion of seawater in lower layers weakens, causing a decrease in salinity. Our results are consistent with the general understanding of the effect of local winds on estuarine circulation (e.g., Wong et al., 1994; Guo and Valle-Levinson, 2008).

Wind remotely affects the estuary by altering sea levels at the estuary mouth (Wong et al., 1994; Guo and Valle-Levinson, 2008; Zhu et al., 2021). The sea level of the Upper Gulf of Thailand, which reaches the river mouth of the CPE, shows a significant sub-tidal variation of as much as 0.4 m during a period of 4–7 days (Figs. 2d and 10a). Although more investigation is needed to fully explain the mechanism of such large sub-tidal sea level variation, the winds over the Upper Gulf of Thailand are likely responsible. Therefore, we used the sub-tidal sea level change recorded at station Pomphrajul to represent the remote wind effects.

Similar to our previous simulations, to investigate the effects of remote winds on the circulation and seawater intrusion in the CPE, we ran these simulations for the period of 1–31 January 2022 with and without the sub-tidal water level data (Fig. 10). Results suggested that the increase in sub-tidal sea level induces an upstream velocity over the entire water column at station C4 (Fig. 10b), followed by an increase of salinity with a time lag of about one day (Fig. 10c), while the decrease of sub-tidal sea level induces an offshore velocity, followed by a decrease of salinity with a time lag of 1 day. This unidirectional current and response of salinity are reported here for the first time for the CPE, and are consistent with reports from other estuaries (Wong et al., 1994; Guo and

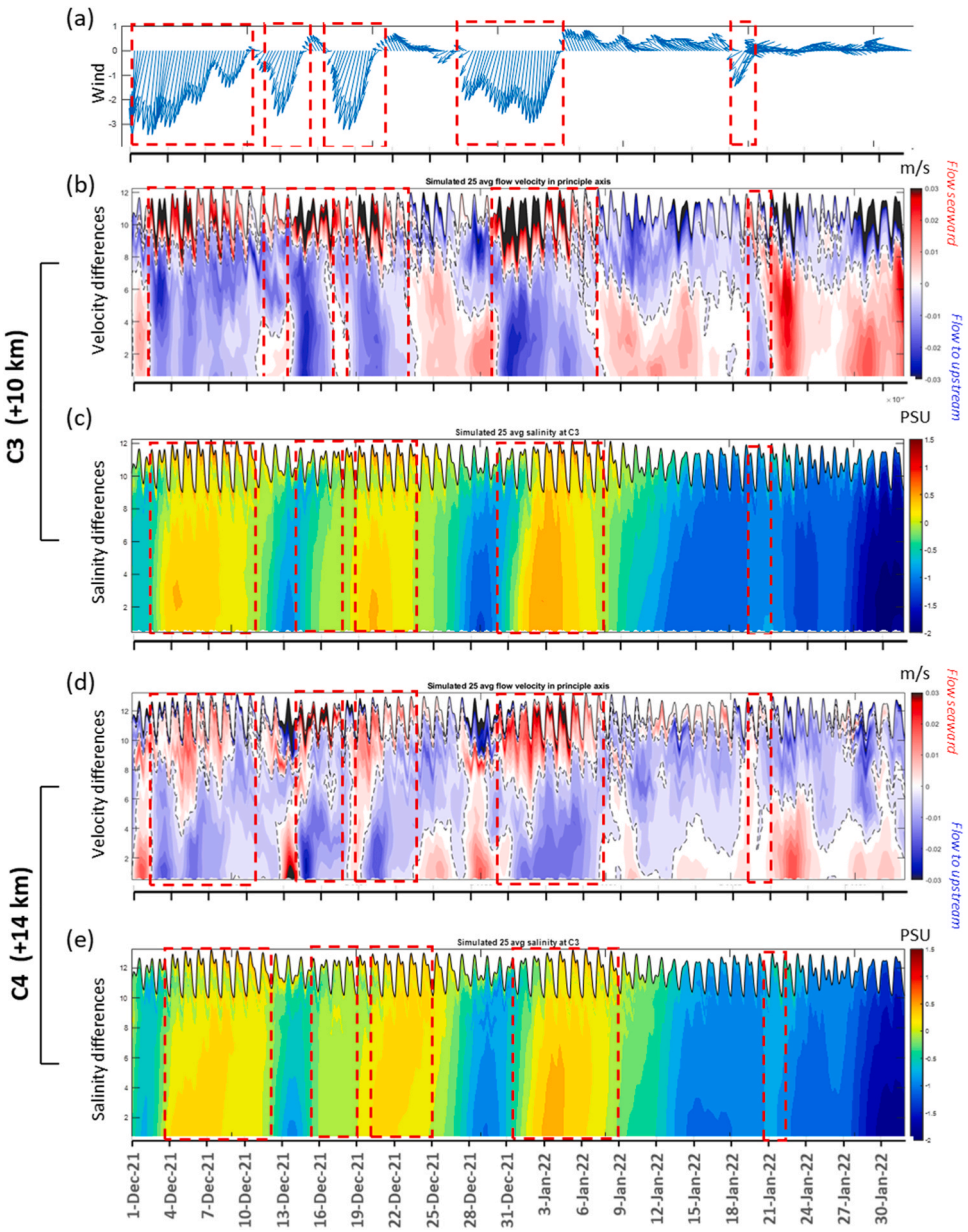

Fig. 9. (a) Wind velocity at station Sriracha. (b) and (c) difference in current velocity in principal direction at station C3 between models with and without winds. Panels (d) and (e) show the same results for station C4. All values are 25-hr low-pass filtered. Blocks bordered by red dashed line highlight periods with dominant down-estuary winds. Black dashed lines in (b) and (d) denote zero current velocity.

Valle-Levinson, 2008).

3.6. Response of the CPE to seasonal variation of sea level outside the CPE

The sea level at the river mouth of the CPE shows a clear seasonal variation (red line in Fig. 2d) that has an amplitude of 0.2 m and is high in winter but low in summer. This seasonal variation has been reported by previous studies (Saramul and Ezer, 2014; Higuchi et al., 2020; Qu et al., 2022). Such seasonal change in sea level is mainly caused by monsoonal winds but with minor contributions by the steric height and atmospheric pressure in the Gulf of Thailand (Higuchi et al., 2020) and South China Sea (Qu et al., 2022).

To determine the influence of sea level on seawater intrusion in the CPE, the model was run both with and without the seasonal variation of sea level outside the river mouth. Note that the models used for calibration and in subsections 3.4 and 3.5 do consider this sea level variation. As shown in Fig. 11, the inclusion of sea level variation can modulate salinity distribution inside the river and affect the seawater intrusion distance, which is short in winter when the sea level is low but is long in summer when the sea level is high. In

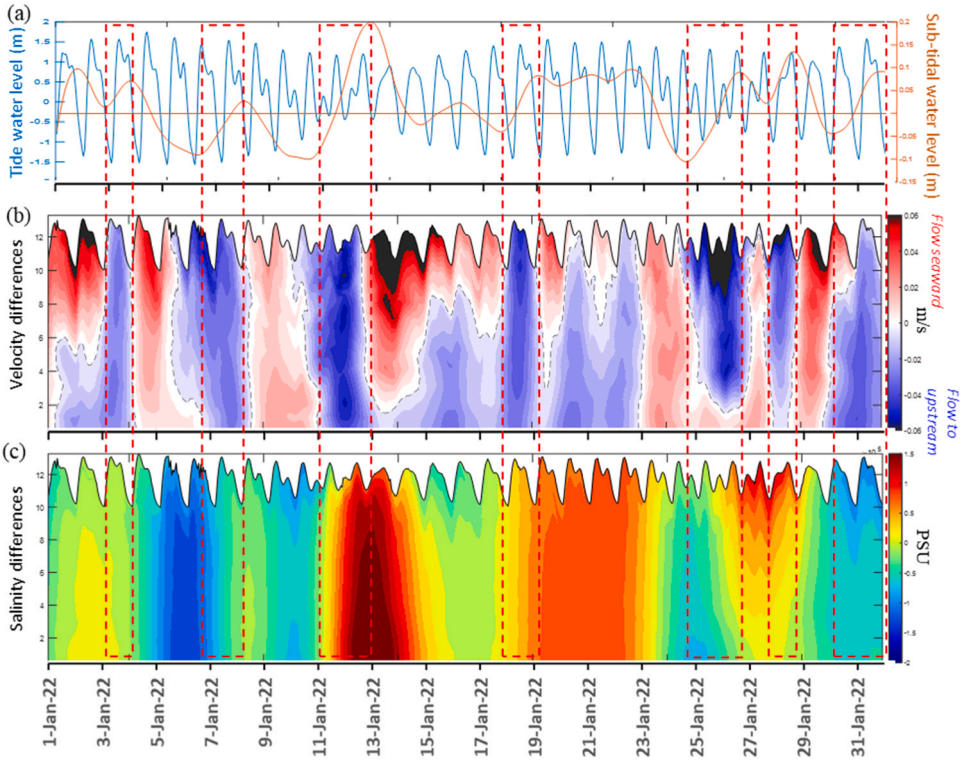

Fig. 10. (a) Tidal (blue line) and sub-tidal (red line) sea level derived from measured data. Note that tidal and subtidal sea levels have different ranges, as shown on left and right sides. Differences in 25-hr low-pass filtered simulation results between models with and without sub-tidal sea level variation for (b) flow velocity in principal direction and (c) salinity. All the values are from station C4. Dashed line in (b) indicates zero flow velocity. Boxes bordered by dashed red lines indicate periods with a significant rising of sub-tidal sea level.

addition, the effect of seasonal sea level variation on seawater intrusion is slightly lower in the dry year than in the wet year. Importantly, the natural seasonal variation of sea levels controlled by monsoon which was found to have amplitude approximately 0.2 m in the Upper Gulf of Thailand can cause a natural alteration in the intrusion distance by about 3–5 km. This has not been previously reported in the CPE or in other estuaries in the same region.

3.7. Responses of the CPE to seasonal freshwater discharge

The water level, circulation and saltwater intrusion in the CPE are greatly affected by the change in freshwater discharge from the Chao Phraya River. Previous section has describe response of the CPE in terms of water level. Salinity and water circulation along the CPE are greatly altered by the change in river discharge as well. Observations show that the saltwater intruded further upstream during the dry year than during the wet year (Fig. 3). Model results also show that the water circulation and salinity distribution in the CPE are different at the end of dry year and that of wet year. To demonstrate this, we present three snapshots of simulation results during the period from October 2020 to March 2021, each with different river discharges (Fig. 12). The CPE saltwater intrusion distance, which is defined as the distance from river mouth to the point with a salinity of 0.25 PSU (Liu et al., 2019), and water circulation are especially sensitive to changes in freshwater discharge. At moderate to high river discharge (> 500 m^3/s), the water within the river flows in one direction toward the sea and the salinity is nearly zero everywhere (Fig. 12a). At low river discharge of about 100–120 m^3/s (an average discharge in the dry season), estuarine circulation occurs from the river mouth to + 60 km and the intrusion distance of seawater sharply increases (Fig. 12b). When the river discharge falls to less than 70–80 m^3/s (minimum discharge in the dry season during the dry year), estuarine circulation is enhanced and the upstream current reaches a distance of 80 km from the river mouth (Fig. 12c). Consequently, the intrusion distance of seawater also can be considered to be 80 km (left panel in Fig. 12). The intrusion distance rapidly increases when the river discharge is less than ~60 m^3/s and reaches 100 km in this case. These results suggest that the estuarine circulation and the intrusion of seawater extend deep into the upstream area of the estuary at the end of a dry year, while they are limited to the areas near the river mouth at the end of a wet (or normal) year. The freshwater discharge rate and saltwater intrusion distance from the river mouth have negative relation with R = - 0.719 *(p-value = 0)*. The freshwater discharge is naturally controlled by rainfall upstream. However, the discharge has been largely regulated and modified by dams, irrigation system and along the river freshwater abstractions in which examples of responses of the estuary will be given in the following section.

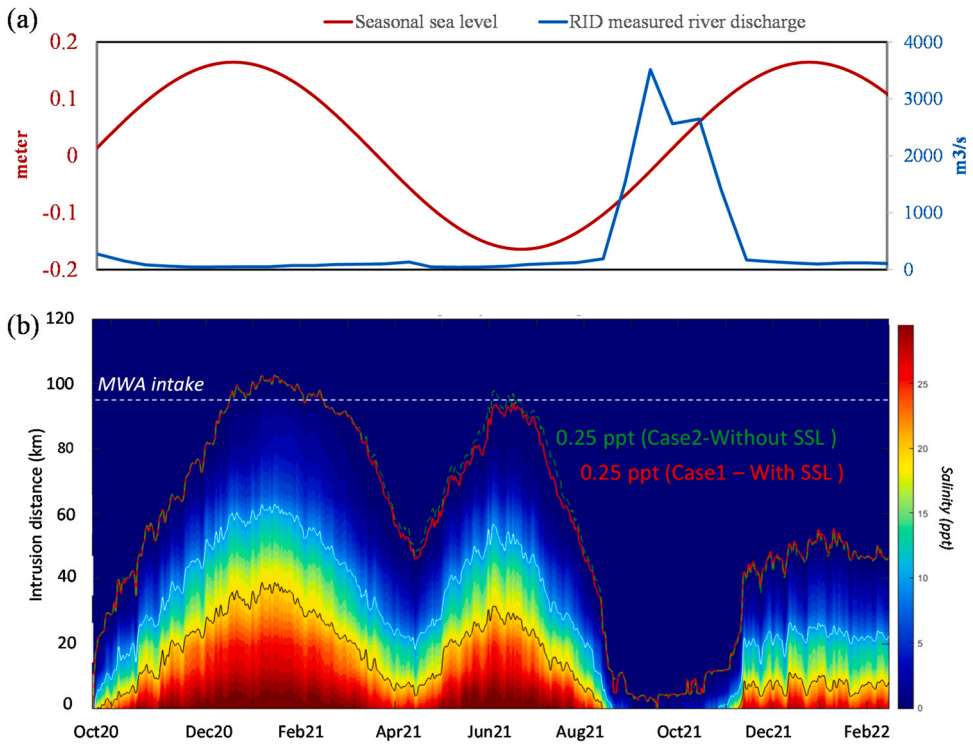

Fig. 11. (a) Seasonal sea level at river mouth and freshwater discharge rate. (b) Color tone indicates surface salinity along the longitudinal axis of the CPE for model that considered variation of seasonal sea level (SSL) outside the CPE. Red line and green line represent contour line of 0.25 ppt from simulations with and without the seasonal variation of sea level, respectively. Location of MWA intake is denoted by a white dashed line in (b).

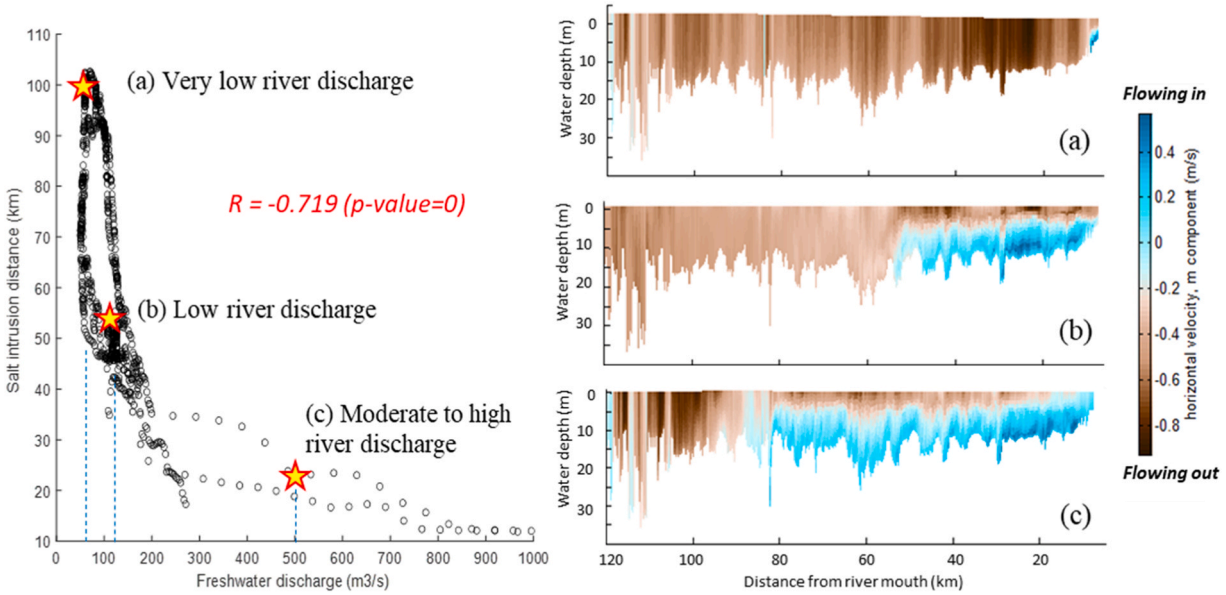

Fig. 12. (left panel) Relationship between freshwater discharge and intrusion distance of seawater from the river mouth. Red stars denote three situations illustrated by the panels at right, which show 25-hr low-pass filtered flow velocity in principal direction along the longitudinal section of the CPE at (a) very low river discharge, (b) low river discharge, and (c) moderate to high river discharge. A negative velocity means downstream.

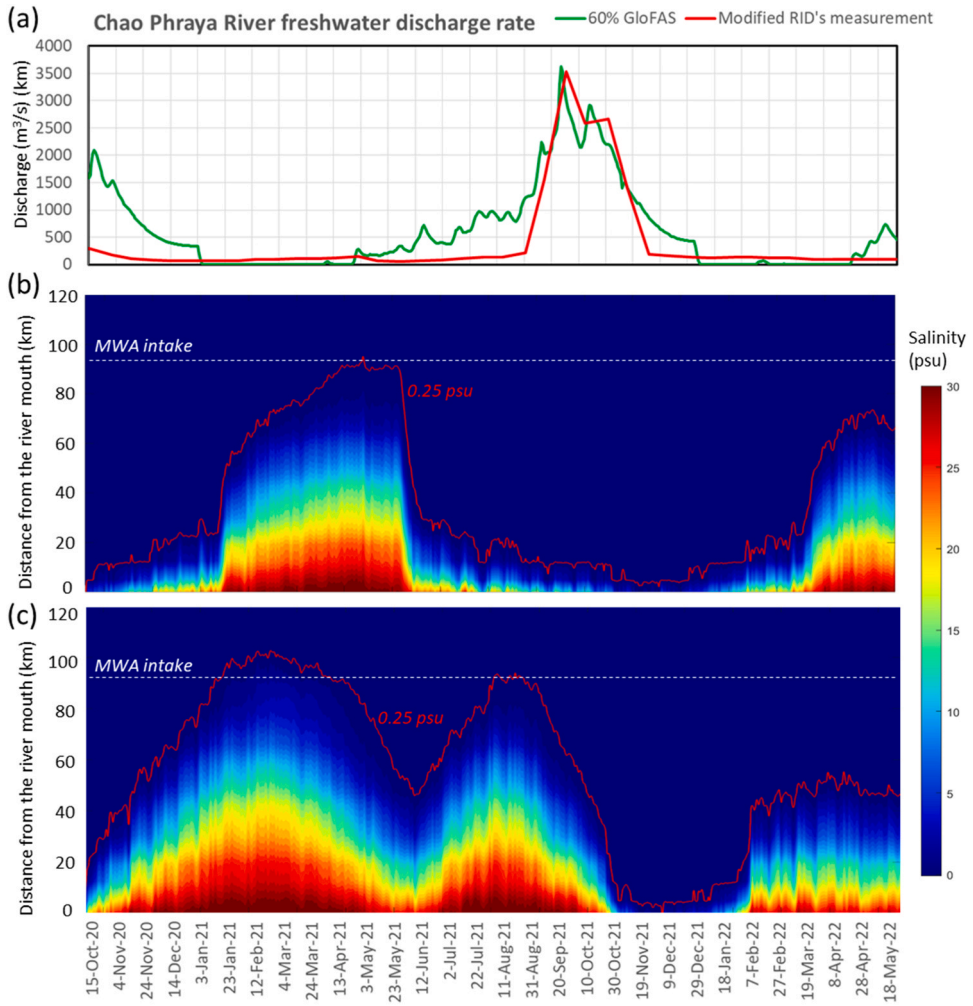

Fig. 13. (a) Comparison between freshwater discharge data from the GloFAS (as free-flowing river and assuming 40% loss) and from the RID measurement (as river with upstream water regulation). Color tones indicate surface salinity along the longitudinal axis of the CPE from model that applied freshwater discharge rate from (b) the GloFAS data and from (c) the RID data. Red lines line represent contour line of 0.25 ppt. Location of MWA intake is denoted by a white dashed line in (b) and (c).

3.8. Responses of the CPE to water regulation and abstraction

Being sensitive to freshwater discharge rate, the CPE has been affected by the upstream water regulation and abstraction from development of water engineering structures (see Table 1). The natural river discharge has been heavily modified and the Chao Phraya River is not free-flowing anymore. To investigate responses of the CPE in terms of the saltwater intrusion, we ran the model with two different scenarios, i.e., first scenario considers no MWA's abstraction and freshwater discharge data from Global Flood Awareness System (GloFAS) and the second scenario considers MWA's abstraction and freshwater discharge from RID measurement. The GloFAS dataset, cover globally, is an estimated daily discharge using the LISFLOOD hydrological model with ERA5 meteorological reanalysis data (Harrigan et al., 2020). Although the GloFAS has incorporate major dams and reservoirs on the modelled river network, it does so in a simplified way.

Fig. 13a compares the natural river discharges derived from the GloFAS data and those measured by the RID. Large discrepancies between them are attributable to water control and some model bias. Also the discrepancies may imply that the freshwater discharge data of the CPE from GloFAS does not affected by upstream water regulation so the GloFAS data can represent the CPE with free-flow condition. The RID data represent current state of the water flow modified by upstream complex water control. At present, an almost steady river discharge of 100 m^3/s is maintained during the dry season as a "base-flow" of the CPE. A portion of the freshwater from rainfall at the beginning and end of the wet season is stored in the upstream dam. This water control results in more rapid changes in the river discharge as compared with the natural flow regime.

Comparison between the Fig. 13b and c, demonstrate a significant changes of spatial and temporal distribution of the salinity along the CPE. Without water control and MWA's abstraction, salinity intrusion occurs only during dry year in 2021 and happened once a

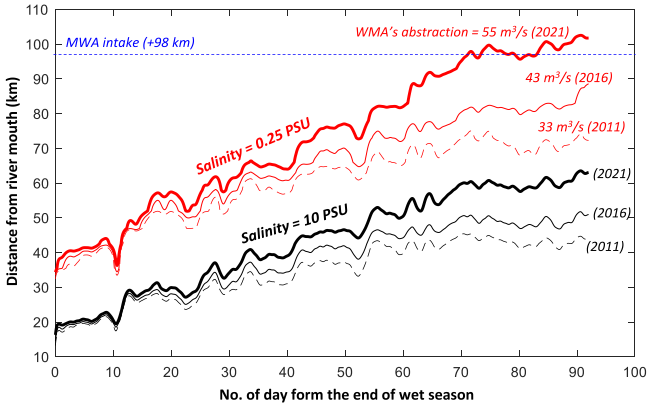

Fig. 14. Temporal variation in the position of surface salinity with 0.25 PSU (red line) and 10 PSU (black line) after the end of the wet season in 2020 (dry year) between simulations with different freshwater abstraction rates by the WMA. The abstraction rates increase at an annual rate of 5% from 2011 to 2021. The WMA intake position is at + 98 km from the estuary mouth.

Table 2
The maximum intrusion distance from river mouth of saltwater with salinity > 0.25 ppt.

Scenario	Wet year (2021)	Dry year (2020)
Free-flow discharge rate without abstraction	22 km	82 km
At present freshwater discharge rate with 2021 abstraction rate (55 m^3/s)	38 km	101 km
At present freshwater discharge rate with 2016 abstraction rate (43 m^3/s)	38 km	91 km
At present freshwater discharge rate with 2011 abstraction rate (33 m^3/s)	38 km	81 km
At present freshwater discharge rate without abstraction	33 km	60 km

year. More severe saltwater intrusion which contaminate freshwater supply of Bangkok occurred twice during the dry year. Not only affects social and economy of the country, increasing salt intrusion modified the fate and transport path of other waterborne materials, e.g., sediment, nutrients, and pollutants (Wei et al., 2022). Saltwater intrusion can change the species abundance and diversity of terrestrial and aquatic communities, affecting the estuary's function and services (e.g., Yin et al., 2008; Unno et al., 2015; Pettit et al., 2016; Xue et al., 2018).

During the wet season, a large amount of freshwater is stored in upstream reservoirs for utilization in the following year. Only excess water during the wet season is freely released into the river. During dry years, the amount of freshwater is limited, and insufficient to meet all of the demand for freshwater. At this time, most of the water is kept in the dams, and only the base-flow is maintained. Molle et al. (2001) reported a possible shortage of freshwater in the dry season for the CPE. Based on projections of water consumption, the study reported serious competition between agriculture and non-agriculture (mainly by the MWA) uses. The authors also suggested that the freshwater available for agriculture in the dry season must be reduced from 4.6 billion m^3 in 2000 to under 3.0 billion m^3 in 2015 because non-agricultural water use was increasing at a rate of 5% per year. Although not shown here, data from the MWA also confirm a 5% increase.

Simulations were then run from conditions at the end of the wet season in the dry year (October 2020 to March 2021) to predict the salinity distribution along the CPE under the same forcing conditions except the freshwater abstract rate at station C22 (location of the MWA's intake), which was set at different historical values: 55 m^3/s in 2021, 43 m^3/s in 2016 and 33 m^3/s in 2011. The calculated salinity distribution along the CPE reflects a strong response to the different freshwater abstraction rates (Fig. 14). Water with salinity higher than the standard for drinking water (<0.25 PSU) reaches the MWA's intake at about 65 days and 90 days after the end of the wet season (October 2020) in the dry year based on the abstraction rate from 2021 (55 m^3/s). Water with salinity this high never reaches the intake location in the simulations of other years, with relatively small abstraction rates. Changes in the position of higher salinity (e.g., 10 PSU) are less sensitive to the abstraction rates. Except for the high abstraction rate in 2021, salinity levels tend to be stable toward the end of the simulations (Fig. 14).

This suggests that anthropogenic modification of freshwater discharge around the heavily populated estuaries can alter the estuarine system. Table 2 summarizes responses of the CPE to different modeling scenarios of river discharge and MWA's water abstraction rates in terms of the saltwater intrusion distance from the river mouth showing that the CPE is highly sensitive to the freshwater discharges factor. Because this factor has not been fully included by many previous studies on estuary dynamics, further examination is necessary to address the effects of changes in freshwater discharge by water engineering structures and freshwater utilization along the river.

4. Conclusions

This study represents the first comprehensive report on the hydrographic features of the CPE, utilizing data from public sources, our own observations, and modeling. The CPE is a partially mixed estuary where the intra- and inter-seasonal hydrodynamics and salt intrusion dynamics are regulated by natural forces and anthropogenic activities. The inter-seasonal dynamics of the CPE are governed by geometry, tides, local winds, sea level fluctuation by remote winds at the seaside, and freshwater discharge in the river. Monsoons induce seasonal changes in river discharge, wind, and seasonal sea level outside the CPE. Regional climate drivers can greatly influence the CPE's dynamics through the inter-annual variation in rainfall that affects river runoff. Human settlement in the CPE and its upstream has modified the freshwater discharge of the river by water regulation and along the river abstraction which alters the dynamics of the estuary in terms of water flow and saltwater intrusion. The interplay between natural and anthropogenic factors as revealed by this study illustrate the importance of considering them together. Complex processes related to estuarine circulation and saltwater intrusion indicate the necessity to use a fine-grid three-dimensional model for the estuary.

Our results suggest that the improvement of freshwater allocation (e.g., by limiting usages from irrigation and cities sector, increase freshwater input by diverging the freshwater from other catchment, etc.) and accurate river discharge measurement are primary ways to effectively manage the saltwater intrusion problem because the saltwater intrusion in the CPE is very sensitive to freshwater discharge. Winds influence saltwater intrusion via both local and remote effects. In addition, because of the clear effects of sea level change on saltwater intrusion and the compelling evidence of relative sea level rise reported in previous studies (Trisirisatayawong et al., 2011; Saramul and Ezer, 2014; Bidorn et al., 2021), we should also consider the sea level change in the Upper Gulf of Thailand.

The limitations of our simulation are the exclusion of the spatial variation in river vegetation and the irrigation system and canals along the river, effects of direct precipitation, seasonal variation in freshwater utilization and its return to the river, agricultural and wastewater drainage and river geometry changes over time. In the future, we want to improve the model for addressing these factors and use our model as a platform for simulations of pollutant transport and water quality in the CPE.

Declaration of Competing Interest

The authors declare that they have no known competing financial interests or personal relationships that could have appeared to influence the work reported in this paper.

Data Availability

The authors do not have permission to share data.

Acknowledgements

The authors convey their appreciations to Thailand's Metropolitan Waterworks Authority, Marine Department and Hydrographic Department for sharing measured data. This work was financially supported by the Office of the Ministry of Higher Education, Science, Research and Innovation; and the Thailand Science Research and Innovation through the Kasetsart University Reinventing University Program 2021. This work was partly supported by the Ministry of Education, Culture, Sports, Science and Technology, Japan (MEXT) to a project on Joint Usage/Research Center–Leading Academia in Marine and Environment Pollution Research (LaMer). X. Guo thanks support from the Environment Research and Technology Development Fund (JPMEERF20212001) of the Environmental Restoration and Conservation Agency of Japan. The authors thank two anonymous reviewers and the editors for their valuable comments which improve the quality and readability of this paper.

Appendix A. Supporting information

Supplementary data associated with this article can be found in the online version at doi:10.1016/j.ejrh.2024.101686.

References

Bidorn, B., Sok, K., Bidorn, K., Burnett, W.C., 2021. An analysis of the factors responsible for the shoreline retreat of the Chao Phraya Delta (Thailand). Sci. Total Environ. 769, 45253. https://doi.org/10.1016/j.scitotenv.2021.145253.

Bowen, M.M., Geyer, W.R., 2003. Salt transport and the time-dependent salt balance of a partially stratified estuary. J. Geophys. Res. 108 (C5), 3158. https://doi.org/10.1029/2001JC001231.

Buranapratheprat, A., Yanagi, T., Niemann, K.O., Matsumura, S., Sojisuporn, P., 2008. Surface chlorophyll-a dynamics in the upper Gulf of Thailand revealed by a coupled hydrodynamic-ecosystem model. J. Oceano 64, 639–656. https://doi.org/10.1007/s10872-008-0054-9.

Cai, W., Sullivan, A., Cowan, T., 2009. Climate change contributes to more frequent consecutive positive Indian Ocean Dipole events. L23704 Geophys. Res. Lett. 36. https://doi.org/10.1029/2009GL040163.

Cai, W., Santoso, A., Collins, M., Dewitte, B., Karamperidou, C., Kug, J.S., Lengaigne, M., McPhaden, M.J., Stuecker, M.F., Taschetto, A.S., Timmermann, A., Wu, L., Yeh, S.W., Wang, G., Ng, B., Jia, F., Yang, Y., Ying, J., Zheng, X.T., Bayr, T., Brown, J.R., Capotondi, A., Cobb, K.M., Gan, B., Geng, T., Ham, Y.G., Jin, F.F., Jo, H. S., Li, X., Lin, X., McGregor, S., Park, J.H., Stein, K., Yang, K., Zhang, L., Zhong, W., 2021. Changing El Niño–Southern Oscillation in a warming climate. Nat. Rev. Earth Environ. 2, 628–644. https://doi.org/10.1038/s43017-021-00199-z.

Changklom, J., Lamchuan, P., Pornprommin, A., 2022. Salinity forecasting on raw water for water supply in the Chao Phraya River. Water 14, 741. https://doi.org/10.3390/w14050741.

Chen, Q., Zhu, J., Lyu, H., Pan, S., Chen, S., 2019. Impacts of topography change on saltwater intrusion over the past decade in the Changjiang Estuary. Estuar., Coast. Shelf Sci. 231, 106469 https://doi.org/10.1016/j.ecss.2019.106469.

Chettanawanit, K., Charoensuk, T., Luangdilok, N., Thanathnphon, W., Mooktaree, A., Lolupiman, T., Kyaw, K.K., Sisomphon, P., 2021. Simulation of water losses for the 1D salinity forecasting model in Chao Phraya River. In Proceedings of the 5th International Conference on Water Resources Engineering, Bangkok, Thailand, 25–26 November 2021.

Crimaldi, M., Lama, G.F.C., 2021. Impacts of riparian plants biomass assessed by UAV-acquired multispectral images on the hydrodynamics of vegetated streams. 29th European Biomass Conference and Exhibition, 26–29 April 2021 Online, 1157–1161. https://dx.doi.org/10.5071/29thEUBCE2021–4AV.3.6.

Deltares, 2017. Simulation of multi-dimensional hydrodynamic flows and transport phenomena, including sediments, Delft3D-FLOW user manual. Delft- Netherland 708 pp..

Ding, Z., Zhu, J., Lyu, H., 2021. Impacts of the Qingcaosha Reservoir on saltwater intrusion in the Changjiang estuary. Anthr. Coasts 4 (1), 17–35. https://doi.org/10.1139/anc-2020-0015.

Dyer, K., 1997. Estuaries, a Physical Introduction, 2nd ed. John Wiley & Sons Ltd. New York, NY, USA, ISBN 0–471-97471–4.

Errico, A., Lama, G.F.C., Francalanci, S., Chirico, G.B., Solari, L., Preti, F., 2019. Validation of global flow resistance models in two experimental drainage channels covered by Phragmites australis (common reed). In Proceedings of the 38th IAHR World Congress-Water Connecting the World, 1313–1321. https://dx.doi.org/10.3850/38WC092019–1215.

Eslami, S., Hoekstra, P., Kernkamp, H., Nguyen Trung, N., Do Duc, D., Tran Quang, T., Februarianto, M., Van Dam, A., van der Vegt, M., 2019a. Flow division dynamics in the mekong delta: application of a ^{1}D–^{2}D coupled model. Water 11, 837. https://doi.org/10.3390/w11040837.

Eslami, S., Hoekstra, P., Nguyen Trung, N., Kantoush, S.A., Van Binh, D., Duc Dung, D., Tran Quang, T., Van der Vegt, M., 2019b. Tidal amplification and salt intrusion in the Mekong Delta driven by anthropogenic sediment starvation. Sci. Rep. 9, 18746 https://doi.org/10.1038/s41598-019-55018-9.

Gong, W., Wang, Y., Jia, J., 2012. The effect of interacting downstream branches on saltwater intrusion in the Modaomen Estuary, China. J. Asian Earth Sci. 45 (4), 223–238. https://doi.org/10.1016/j.jseaes.2011.11.001.

Gong, W., Zhang, G., Zhang, H., Yu, X., Zhu, L., Li, S., 2022. The effects of mouth bar on salt intrusion in a partially mixed estuary (C). J. Hydrol. 612, 128261. https://doi.org/10.1016/j.jhydrol.2022.128261.

Guo, X., Valle-Levinson, A., 2007. Tidal effects on estuarine circulation and outflow plume in the Chesapeake Bay. Cont. Shelf Res. 27 (1), 20–42. https://doi.org/10.1016/j.csr.2006.08.009.

Guo, X., Valle-Levinson, A., 2008. Wind effects on the lateral structure of density-driven circulation in Chesapeake Bay. Cont. Shelf Res. 28 (17), 2450–2471. https://doi.org/10.1016/j.csr.2006.08.009.

Harrigan, S., Zsoter, E., Alfieri, L., Prudhomme, C., Salamon, P., Wetterhall, F., Barnard, C., Cloke, H., Pappenberger, F., 2020. GloFAS-ERA5 operational global river discharge reanalysis 1979—present. Earth Syst. Sci. Data 12 (3), 2043–2060. https://doi.org/10.5194/essd-12-2043-2020.

Higuchi, M., Anongponyoskun, M., Phaksopa, J., Onishi, H., 2020. Influence of monsoon-forced Ekman transport on sea surface height in the Gulf of Thailand. Agric. Nat. Resour. 54 (2), 205–210. https://doi.org/10.34044/j.anres.2020.54.2.12.

Horiuchi, Y., Matsuura, T., Tebakari, T., Wongsa, S., 2020. Meta-analysis of Water Quality Characteristics in the Lower Chaophraya River, Thailand. In Proceedings of the 22nd IAHR-APD Congress 2020, Sapporo, Japan, 14–17 September 2020.

Jaroenongard, C., Babel, M.S., Shrestha, S., Weesakul, S., Nitivattananon, V., Khadka, D., 2021. Projecting relative sea level rise under climate change at the Phrachula Chomklao Fort Tide Gauge in the Upper Gulf of Thailand. Water 13 (12), 1702. https://doi.org/10.3390/w13121702.

Liu, B., Peng, S., Liao, Y., Wang, H., 2019. The characteristics and causes of increasingly severe saltwater intrusion in Pearl River Estuary. Estuar., Coast. Shelf Sci. 220, 54–63. https://doi.org/10.1016/j.ecss.2019.02.041.

Molle, F., Chompadist, C., Srijantr, T., Keawkulaya, J., 2001. Dry-season water allocation and management in the Chao Phraya Delta. https://doi.org/10.13140/2.1.2412.4482.

Payo-Payo, M., Bricheno, L.M., Dijkstra, Y.M., Cheng, W., Gong, W., Amoudry, L.O., 2022. Multiscale temporal response of salt intrusion to transient river and ocean forcing. J. Geophys. Res.: Oceans 127, e2021JC017523. https://doi.org/10.1029/2021JC017523.

Pein, J., Valle-Levinson, A., Stanev, E.V., 2018. Secondary circulation asymmetry in a meandering, partially stratified estuary. J. Geophys. Res.: Oceans 123, 1670–1683. https://doi.org/10.1002/2016JC012623.

Pettit, N.E., Bayliss, P., Bartollo, R., 2016. Dynamics of plant communities and the impact of saltwater intrusion on the floodplains of Kakadu National Park. Mar. Freshw. Res. 69 (7) https://doi.org/10.1071/MF16148.

Phan-Van, T., Nguyen-Ngoc-Bich, P., Ngo-Duc, T., Vu-Minh, T., Le, P.V.V., Trinh-Tuan, L., Nguyen-Thi, T., Pham-Thanh, H., Tran-Quang, D., 2022. Drought over Southeast Asia and Its Association with Large-Scale Drivers. J. Clim. 35 (15), 4959–4978. https://doi.org/10.1175/JCLI-D-21-0770.1.

Prandle, D., 1985. On salinity regimes and the vertical structure of residual flows in narrow tidal estuaries. Estuar. Coast. Shelf Sci. 20, 615–635. https://doi.org/10.1016/0272-7714(85)90111-8.

Prandle, D., 2006. Dynamical controls on estuarine bathymetry: assessment against UK database. Estuar. Coast. Shelf Sci. 68 (1–2), 282–288. https://doi.org/10.1016/j.ecss.2006.02.009.

Pritchard, D.W., 1955. Estuarine Circulation patterns. Proceeding of American Society of Civil Engineering 81, No. 717., 1–11. https://doi.org/10.1007/978–94-017–8801-4_176.

Qu, Y., Jevrejeva, S., Williams, J., Moore, J.C., 2022. Drivers for seasonal variability in sea level around the China seas. Glob. Planet. Change 23, 103819. https://doi.org/10.1016/j.gloplacha.2022.103819.

Ralston, D.K., 2022. Impacts of storm surge barriers on drag, mixing, and exchange flow in a partially mixed estuary. J. Geophys. Res.: Oceans 127, e2021JC018246. https://doi.org/10.1029/2021JC018246.

Saito, Y., 2001. Deltas in Southeast and East Asia: Their evolution and current problems. In Mimura, N. and Yokoki, H., eds., Global Change and Asia Pacific Coasts. Proceedings of APN/SURVAS/LOICZ Joint Conference on Coastal Impacts of Climate Change and Adaptation in the Asia-Pacific Region, APN, Kobe, Japan, November 14–16, 2000, p. 185–191.

Saramul, S., Ezer, T., 2014. Spatial variations of sea level along the coast of Thailand: Impacts of extreme land subsidence, earthquakes and the seasonal monsoon. Glob. Planet. Change 122, 70–81. https://doi.org/10.1016/j.gloplacha.2014.08.012.

Shen, Y., Jia, H., Li, C., Tang, J., 2018. Numerical simulation of saltwater intrusion and storm surge effects of reclamation in Pearl River Estuary, China. Appl. Ocean Res. 79, 101–112. https://doi.org/10.1016/j.apor.2018.07.013.

Simpson, J.H., Brown, J., Matthews, J., Allen, G., 1990. Tidal straining, density currents, and stirring in the control of estuarine stratification. Estuaries 13, 125–132. https://doi.org/10.2307/1351581.

Sirisup S., Saengnin, N., Tomkatoke, S., 2014. Simulation of estuarine hydrological characteristic: A Case Study of the Lower Chao Praya River 25–1, 21–30. (In Thai, with English abstract).

Smith, S.D., Banke, E.G., 1975. Variation of the sea surface drag coefficient with wind speed. Q. J. R. Meteorol. Soc. 101, 665–673. https://doi.org/10.1002/qj.49710142920.

Trisirisatayawong, I., Naeije, M., Simons, W., Fenoglio-Marc, L., 2011. Sea level change in the Gulf of Thailand from GPS-corrected tide gauge data and multi-satellite altimetry. Glob. Planet. Change 76 (3-4), 137–151. https://doi.org/10.1016/j.gloplacha.2010.12.010.

Unno, T., Kim, J., Kim, Y., Nguyen, S.G., Guevarra, R.B., Kim, G.P., Sadowsky, M.J., 2015. Influence of seawater intrusion on microbial communities in groundwater. Sci. Total Environ. 532, 337–343. https://doi.org/10.1016/j.scitotenv.2015.05.111.

Vongvisesssomjai, S., Chatanantavet, P., 2006. Analytical model of interaction of tide and river flow. Songklanakarin J. Sci. Technol. 28-6, 1149–1160.

Vossen, B. van, 2000. Horizontal Large Eddy simulations; evaluation of flow computations with Delft3D-FLOW. Tech. Rep. MEAH-197, WL | Delft Hydraulics, Delft, The Netherlands.

Wang, A., Guo, X., Morimoto, A., Maetani, K., Tanoue, R., Tong-U-Dom, S., Buranapratheprat, A., 2021. Transport and dilution of fluvial antibiotic in the Upper Gulf of Thailand. Environ. Pollut. 288, 117779 https://doi.org/10.1016/j.envpol.2021.117779.

Wei, X., Williams, M.E., Brown, J.M., Thorne, P.D., Amoudry, L.O., 2022. Salt intrusion as a function of estuary length in periodically weakly stratified estuaries. Geophys. Res. Lett. 49, e2022GL099082 https://doi.org/10.1029/2022GL099082.

Wong, K.C., 1994. On the nature of transverse variability in a coastal plain estuary. J. Geophys. Res. 99 (C7), 14209–14222. https://doi.org/10.1029/94JC00861.

Wongsa, S., 2015. Impact of climate change on water resources management in the lower Chao Phraya Basin, Thailand. J. Geosci. Environ. Prot. 3 (10), 53. https://doi.org/10.4236/gep.2015.310009.

Xue, L., Li, X., Zhang, Q., Yan, Z., Ding, W., Huang, X., Yin, Q., 2018. Elevated salinity and inundation will facilitate the spread of invasive Spartina alterniflora, in the Yangtze. River Estuary, China. J. Exp. Mar. Biol. Ecol. 506, 144–154. https://doi.org/10.1016/j.jembe.2018.06.008.

Yang, W., Wei, H., Zhao, L., 2017. Observations of tidal straining within two different ocean environments in the East China Sea: stratification and near-bottom turbulence. J. Geophys. Res.: Oceans 122, 8876–8893. https://doi.org/10.1002/2017JC012924.

Yin, K., Harrison, P.J., 2008. Nitrogen over enrichment in subtropical Pearl River Estuarine coastal waters: possible causes and consequences. Continetal Shelf Res. 28 (12), 1435–1442. https://doi.org/10.1016/j.csr.2007.07.010.

Zhang, Q., Xu, C.Y., Chen, Y.D., 2010. Wavelet-based characterization of water level behaviors in the Pearl River estuary, China. Stoch. Environ. Res. Risk Assess. 24, 81–92. https://doi.org/10.1007/s00477-008-0302-y.

Zhu, J., Cheng, X., Li, L., Wu, H., Gu, J., Lyu, H., 2020. Dynamic mechanism of an extremely severe saltwater intrusion in the Changjiang estuary in February 2014. Hydrol. Earth Syst. Sci. 24, 5043–5056. https://doi.org/10.5194/hess-24-5043-2020.